Available online at www.sciencedirect.com
ScienceDirect
Journal of Organometallic Chemistry 692 (2007) 1377–1391
Journal of Organometallic Chemistry
www.elsevier.com/locate/jorganchem

Photophysical properties and computational investigations of tricarbonylrhenium(I)[2-(4-methylpyridin-2-yl)benzo[*d*]-X-azole]L and tricarbonylrhenium(I)[2-(benzo[*d*]-X-azol-2-yl)-4-methylquinoline]L derivatives (X = N–CH_3, O, or S; L = Cl^-, pyridine)

Andrea Albertino [a], Claudio Garino [a], Simona Ghiani [a], Roberto Gobetto [a,*], Carlo Nervi [a], Luca Salassa [a], Edward Rosenberg [b], Ayesha Sharmin [b], Guido Viscardi [c], Roberto Buscaino [c], Gianluca Croce [d], Marco Milanesio [d]

[a] *Dipartimento di Chimica IFM and MI Centers of Excellence, Università di Torino, Via P. Giuria 7, I-10125 Torino, Italy*
[b] *Department of Chemistry, University of Montana, Missoula, MT 59812, USA*
[c] *Dipartimento di Chimica Generale ed Organica Applicata and NIS Centre of Excellence, Università di Torino, Corso M. D'Azeglio 48, 10125 Torino, Italy*
[d] *Dipartimento di Scienze e Tecnologie Avanzate and NANOSISTEMI Centre of Excellence, Università del Piemonte Orientale "A. Avogadro", Via Bellini 25/G, 15100 Alessandria, Italy*

Received 27 September 2006; received in revised form 2 November 2006; accepted 2 November 2006
Available online 11 November 2006

Abstract

We report a combined experimental and computational study of new rhenium tricarbonyl complexes based on the bidentate heterocyclic N–N ligands 2-(4-methylpyridin-2-yl)benzo[*d*]-X-azole (X = N–CH_3, O, or S) and 2-(benzo[*d*]-X-azol-2-yl)-4-methylquinoline (X = N–CH_3, O, or S). Two sets of complexes are reported. Chloro complexes, described by the general formula $Re(CO)_3$[2-(4-methylpyridin-2-yl)benzo[*d*]-X-azole]Cl (X = N–CH_3, **1**; X = O, **2**; X = S, **3**) and $Re(CO)_3$[2-(benzo[*d*]-X-azol-2-yl)-4-methylquinoline]Cl (X = N–CH_3, **4**; X = O, **5**; X = S, **6**) were synthesized heating at reflux $Re(CO)_5Cl$ with the appropriate N–N ligand in toluene. The corresponding pyridine set {$Re(CO)_3$[2-(4-methylpyridin-2-yl)benzo-X-azole]py}PF_6 (X = N–CH_3, **7**; X = O, **8**; X = S, **9**) and {$Re(CO)_3$[2-(benzo[*d*]-X-azol-2-yl)-4-methylquinoline]py}PF_6 (X = N–CH_3, **10**; X = O, **11**; X = S, **12**) was synthesized by halide abstraction with silver nitrate of **1**–**6** followed by heating in pyridine and isolated as their hexafluorophosphate salts. All complexes have been fully characterized by IR, NMR, electrochemical techniques and luminescence. The crystal structures of **1** and **7** were obtained by X-ray diffraction. DFT and time-dependent (TD) DFT calculations were carried out for investigating the effect of the organic ligand on the optical properties and electronic structure of the reported complexes.

Keywords: Electrochemistry; Luminescence; Rhenium; Heterocyclic bidentate ligands; Excited-state calculations; DFT

1. Introduction

A large number of metal complexes that exhibit charge transfer bands have been synthesized in the last few years for their fundamental and applicative properties. Their particular photophysical properties (luminescence, photochemistry, electrochemiluminescence) have been applied to several branches of chemistry [1–3], biochemistry [4], and solar technology [5–7]. Transition metal complexes having luminescent properties have been employed in molecular recognition [8–10], investigations of electron transfer, energy transfer in biological systems and in the design of new sensors for trace pollutants or contaminants [11–13]. We are interested in developing novel transition metal complexes as luminescent [14] and electrochemiluminescent [15]

* Corresponding author. Tel.: +39 011 670 7523; fax: +39 011 6707855.
E-mail address: roberto.gobetto@unito.it (R. Gobetto).

0022-328X/$ - see front matter © 2006 Elsevier B.V. All rights reserved.
doi:10.1016/j.jorganchem.2006.11.004

probes for biological applications. The design of a good candidate for luminescence applications requires a careful choice of both the metal and the ligands because only the appropriate combination of π^*-orbitals on the organic ligands with the d-orbitals associated with the metal results in new transitions involving charge transfer. In general the d–d states must be at higher energies with respect to the metal-to-ligand charge transfer states. This is accomplished by increasing the crystal field strength with appropriate ancillary ligands (CO, CN^-, PPh_3), in addition to the diimine electron acceptor ligand, and by the choice of metals in the second and third row.

Even though ruthenium-based complexes are more common, there is significant interest in rhenium tricarbonyl derivatives [16–19]. In particular, rhenium tricarbonyl derivatives are characterized by high chemical and photochemical stability with respect to related ruthenium complexes. $Re(CO)_5Cl$ represents an excellent starting material for the synthesis of luminescent complexes, because of the accessibility of synthetic procedures for obtaining high yields of $Re(N–N)(CO)_3L$ derivatives (where N–N is a bidentate ligand and L = halogen or N base). The control of photophysical properties for these complexes can be achieved by two methods: (i) by using a ligand with different ligand-field strength to adjust the energy levels of the metal-centered dπ orbitals, and (ii) by using functional groups which modulate the electron donor or acceptor properties of the ligands. Diimine ligands allow the control of the charge transfer emission energy. $Re(CO)_3$ derivatives show significant Stokes' shifts capable of minimizing the self-quenching effects frequently encountered in multiple labeling of biomolecules with fluorescent organic dyes. The longer emission lifetimes compared to organic fluorophores are useful in time-resolved detection techniques allowing the suppression of the interference of short lifetime bio-macromolecule autofluorescence [16]. Rhenium(I) polypyridine complexes have been also employed as promising candidates for biological applications as anisotropy probes for protein hydrodynamics [17–19].

The bidentate diimine ligand 2-(pyridin-2-yl)benzo-X-azole (X = N-R, O, S) has a long history in coordination chemistry [20,21]. More recently, studies of $Ru(bpy)_2$ [15] and $Re(CO)_3L$ ($L = Cl^-$, Br^-, $CF_3SO_3^-$, CH_3CN) complexes with these ligands have focused on their structural, photoelectric, photophysical and redox properties with applications in photoelectric devices and supramolecular photochemistry in mind [22–26]. Based on this previous work we have become interested in developing this ligand–metal complex system for application in biomolecular structure and dynamics as biosensors, an area that has received some attention in the case of the $Re(bpy)(CO)_3L$ complexes [1]. We found, however, that a detailed understanding of the photophysical and redox properties of the series of complexes Re[2-(pyridin-2-yl)benzo-X-azole] $(CO)_3L$ needed further investigation.

We report here a combined experimental and computational study of this class of rhenium tricarbonyl complexes based on the bidentate heterocyclic ligands 2-(4-methylpyridin-2-yl)benzo[*d*]-X-azole (mpbX), where X = N–CH_3 (mpbN), O (mpbO) or S (mpbS), and 2-(benzo[*d*]-X-azol-2-yl)-4-methylquinoline (mqbX), where X = N–CH_3 (mqbN), O (mqbO) or S (mqbS). The use of these ligands in place of the usual diimine ligands such as phenanthroline or bipyridine provides the opportunity to tune the electronic properties of the complexes by changing the heteroatom in the benzo-X-azole ring. In addition, the C–CH_3 and N–CH_3 groups are anchoring sites for bioconjugation. In particular, the benzimidazole provides both groups, whose different reactivity allows a tuned bio-functionalization. Besides, the low symmetry of these complexes holds out the promise of a high degree of fundamental anisotropy and the associated polarized emission [1]. Taken together these purported properties could prove extremely useful for applications in biomolecular structure and dynamics. In this study we report the attempts to model singlet and triplet excited-states of luminescent $Re(N–N)(CO)_3L$ derivatives using the time-dependent density functional theory (TDDFT) method along with the polarizable continuum model (PCM) to model solvent effects for the gas phase computational results. This study is focused on the electronic effects displayed by the different benzimidazole ligands on the UV–Vis and geometric properties of the synthesized rhenium complexes.

2. Results and discussion

The complexes were synthesized by the pathway shown in Scheme 1. The strongly bound Cl atom was removed by reaction of **1**–**6** with $AgNO_3$ in acetonitrile. Solid AgCl was filtered off, and compounds **7**–**12** were finally obtained replacing CH_3CN by pyridine. The PF_6^- salt complexes **7**–**12** were obtained by adding NH_4PF_6 to precipitate the products.

All the newly synthesized complexes were characterized by ^1H NMR, ^{13}C NMR, IR, and electrochemical techniques. They show three *ν*(CO) stretches in the IR spectra, typical of Re(I) diimine tricarbonyl complexes with carbonyls arranged in a facial configuration [27]. The structure of complexes **1** and **7** were determined by X-ray crystallography.

2.1. Solid state structures of complexes *1* and *7*

The structures of **1** and **7** are illustrated in Figs. 1 and 2. The crystallographic data are given in Table 1 and selected distances and bond angles are given in Tables 2 and 3, respectively. The two crystal structures belong to the centrosymmetric $P\bar{1}$ triclinic space group and the ligand arrangement around the rhenium atom is similar for the two structures. Their crystal packing features are almost identical. The presence in **7** of the pyridine group and anion PF_6^- causes some changes in the lattice parameters with an increase in the cell volume. The crystal packing is clearly driven by the π–π stacking between benzo-X-azole

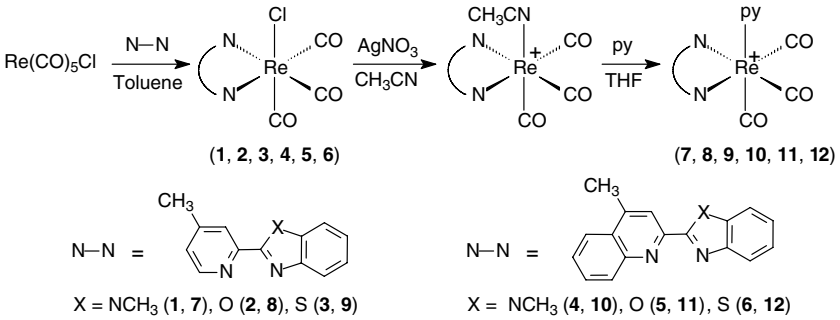

Scheme 1.

moieties. The presence in **7** of the anion PF_6^- does not influence the π–π stacking effect. In fact, only a small shift between the parallel plains is recorded and their distance increases from 3.75 Å to 4.00 Å. The overall structure of both complexes can be considered as a distorted octahedral with the largest deviations from the expected 90° bond angles coming from the bite angles of the pyrid-2-yl-2-benzimidazole ligands. The bite angles are 74.26(0.41)° and 74.05(0.14)°, for **1** and **7**, respectively, and are similar to the ones previously reported for the related Re(pyrid-2-yl-2-benzo-X-azole)$(CO)_3$L complexes (X = N–R, S; L = Cl^-, CH_3CN; 71.2–75.1°) [22–24]. The C(1)–Re–C(2) and C(1)–Re–C(3) bond angles are significantly smaller in **1** compared with **7** being 85.80(0.64)° and 85.8(0.66)° and 88.44(0.25)° and 88.12(0.22)° in **1** and **7**, respectively. However, these values fall within the overall range observed for these angles (84.1–95.9°) in both the cationic and neutral Re(pyrid-2-yl-2-benzo-X-azole)$(CO)_3$L (X = N–R, S; L = Cl^-, CH_3CN), where an analogous increase in bond angle is observed going from a neutral to a cationic species [22–24]. There is a shortening of the Re–C(1) bond on going from **1** to **7** (1.981(16)–1.926(7) Å) and a corresponding increase in the C(1)–O(1) bond length (1.069(21)–1.145(7) Å) while the corresponding bond lengths for the other two CO groups remain essentially constant when averaged (Table 2). This is undoubtedly due to the stronger σ-donor ability of pyridine relative to chloride, which most strongly affects the carbonyl *trans* to pyridine. Significantly, this same shortening of the *trans*-Re–CO bond is not observed going from the neutral triflate complex to the corresponding cationic acetonitrile complex in the series Re(pyrid-2-yl-2-benzothiazole)$(CO)_3$L, where these bond lengths are all in the range 1.910–1.931 Å [22]. This of course reflects the weaker σ-donor ability of acetonitrile relative to pyridine. As for all the previously reported complexes, the Re–N(2)(benzimidazole) bond (2.168(11) Å and 2.155(3) Å) is significantly shorter than the Re–N(1)(pyridine) bond (2.177(11) Å and 2.192(3) Å) in **1** and **7** [23,24]. The pyridine ring in **7** lies in a plane perpendicular to the pyrid-2-yl-2-benzimidazole ring and bisects the C–C bond connecting the two heterocycles. An interesting difference between the two structures is the distortion from planarity of the mpbX group in **1**. The origin of this distortion is not clear but it should be noted that the chlorine atom is slightly bent towards the ring (Fig. 1). The angle between the planes of the benzo and of the azole moiety is in fact

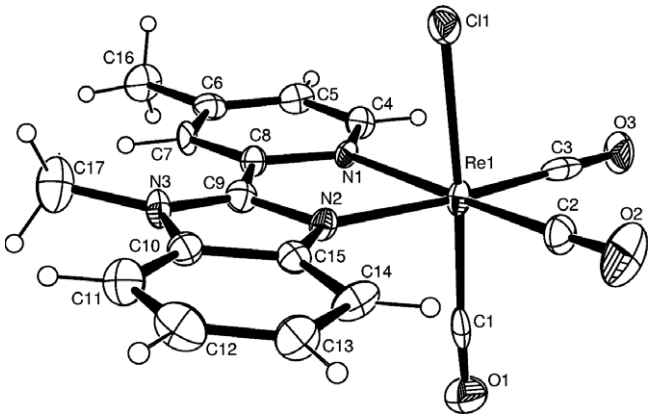

Fig. 1. Solid state structure of complex **1** showing the adopted labeling scheme, with displacement ellipsoids drawn at 30% probability.

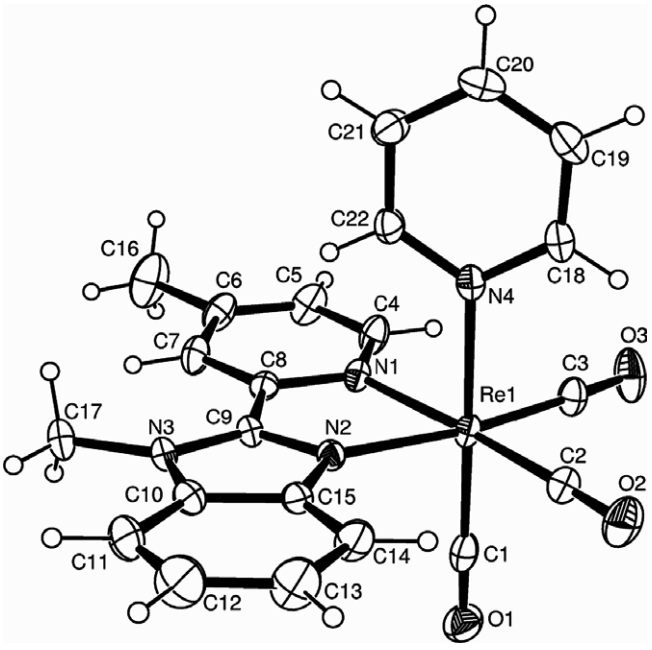

Fig. 2. Solid state structure of compound **7** showing the adopted labeling scheme, with displacement ellipsoids drawn at 30% probability. The anion PF_6^- in **7** is not shown for sake of clarity.

Table 1
Summary of crystal data and structure refinement for complexes **1** and **7**

Compound	**1**	**7**
Empirical formula	$C_{17}H_{13}ClN_3O_3Re$	$C_{22}H_{18}F_6N_4O_3PRe$
Formula weight	528.955	717.57
Temperature (K)		298(2)
Wavelength (Å)		0.71069
Crystal system	$P\bar{1}$	$P\bar{1}$
Space group	Triclinic	Triclinic
Unit cell dimensions		
a (Å)	8.094(3)	9.326(1)
b (Å)	8.249(3)	10.678(1)
c (Å)	13.603(4)	13.739(1)
α (°)	81.86(1)	76.997(5)
β (°)	80.97(1)	81.113(4)
γ (°)	80.09(1)	67.491(6)
Volume (Å^3)	877.4(4)	1228.0(1)
Z	2	2
D_{calc} (Mg/m^3)	2.002	1.941
Absorption coefficient (mm^{-1})	7.10	5.091
$F(000)$	504	692
Crystal size (mm)	$0.30 \times 0.28 \times 0.20$	$0.40 \times 0.30 \times 0.20$
θ Range for data collection (°)	4.93–23.24	4.58–30.28
Index ranges	$-8 \leqslant h \leqslant 8$, $-9 \leqslant k \leqslant 8$, $-15 \leqslant l \leqslant 15$	$-13 \leqslant h \leqslant 13$, $-14 \leqslant k \leqslant 14$, $-18 \leqslant l \leqslant 18$
Reflections collected	8049	18 434
Independent reflections	2287	5892
Completeness to $\theta = 23.24°$ (%)	99	99.9
Refinement method		Full-matrix least-squares on F^2
Data/restraints/parameters	2287/0/226	5892/0/334
Goodness-of-fit on F^2	1.138	1.063
Final R indices [$I > 2\sigma(I)$]	$R_1 = 0.0595$, $wR_2 = 0.1539$	$R_1 = 0.0399$, $wR_2 = 0.0737$
R indices (all data)	$R_1 = 0.0576$, $wR_2 = 0.1517$	$R_1 = 0.0349$, $wR_2 = 0.0698$
Largest difference in peak and hole (e Å^{-3})	3.349 and −2.080	3.392 and −1.694

−4.67° and −0.87° for **1** and **7**, respectively. This causes a significant difference in the torsion angle N(3)–C(9)–C(8)–C(7), which might affect the aromatic character of the mpbX group in **1**.

2.2. Electrochemical studies

The electrochemical properties of complexes **1**–**12** were studied by cyclic voltammetry (CV) and square wave voltammetry (SWV) in acetonitrile solutions. Potentials were reported versus the ferrocene/ferrocenium redox couple, used as an internal standard.

All rhenium complexes show a first, 1e electrochemically and chemically reversible reduction. Plots of the cathodic peak currents versus the square root of the scan rates are linear. Cathodic to anodic peak separations, namely $\Delta E_p = |E_p^c - E_p^a| \approx 80$–$120$ mV, are almost constant with

Table 2
Selected bond lengths (Å) for complexes **1** and **7**

Atom 1	Atom 2	**1**	**7**
Re1	C1	1.981(16)	1.926(7)
Re1	C2	1.937(16)	1.927(5)
Re1	C3	1.904(16)	1.925(4)
Re1	N1	2.177(11)	2.192(3)
Re1	N2	2.168(11)	2.155(3)
Re1	Cl1, N4	2.497(4)	2.220(4)
C1	O1	1.069(21)	1.145(7)
C2	O2	1.140(22)	1.149(6)
C3	O3	1.174(20)	1.146(5)
N3	C17	1.476(23)	1.470(6)
C8	C9	1.468(18)	1.469(6)
C8	N1	1.396(18)	1.381(5)
C9	N2	1.355(18)	1.361(5)
N1	C4	1.321(16)	1.336(5)
N2	C15	1.360(16)	1.383(6)

Table 3
Selected angles (°) for complexes **1** and **7**[a]

Atom 1	Atom 2	Atom 3	**1**	**7**
Re1	C1	O1	175.92(1.54)	178.91(0.56)
Re1	C2	O2	177.61(1.57)	178.33(0.46)
Re1	C3	O3	177.51(1.38)	177.51(0.49)
C3	Re1	C2	85.81(0.66)	88.12(0.22)
C3	Re1	C1	85.80(0.64)	89.44(0.25)
C2	Re1	N2	100.49(0.57)	100.60(0.19)
C2	Re1	N1	173.44(0.57)	174.61(0.18)
C3	Re1	N2	173.51(0.57)	170.94(0.19)
C3	Re1	N1	99.35(0.56)	97.20(0.19)
C1	Re1	N2	92.55(0.53)	93.27(0.21)
C1	Re1	N1	94.18(0.52)	32.59(0.19)
N2	Re1	N1	74.26(0.41)	74.05(.14)
N2	Re1	Cl1, N4	83.97(0.29)	86.47(0.15)
N1	Re1	Cl1, N4	83.28(0.28)	86.63(0.15)
C1	Re1	Cl1, N4	176.14(0.48)	179.21(0.22)
C2	Re1	Cl1, N4	92.17(0.48)	92.50(0.20)
C3	Re1	Cl1, N4	94.27(0.46)	90.70(0.20)

[a] Numbers in parentheses are average standard deviations.

the scan rate in the range from 0.1 to 10 V/s. Similar values were obtained for the ferrocene redox couple under the same conditions.

The subsequent 1e reduction process is chemically irreversible for all compounds (Table 4). For compounds **6**, **11** and **12**, further reversible reductions are observed at −1.97, −2.01 and −1.97 V, respectively. A reversible process after a chemically irreversible peak almost certainly indicates that the reduction process is followed by a homogeneous chemical reaction generating a new species, which is reversibly reduced. In fact, adding a small amount of the corresponding free ligand in the solutions of **6, 11** and **12**, respectively, an increase of the reversible peak heights is observed at −1.97, −2.01, and −1.97 V, respectively. Thus, the introduction of two electrons onto the rhenium centers leads to the release of the free organic ligand in the case of **6, 11** and **12**. Compound **7** shows also a 1e reversible oxidation process centered at $E^{\circ}(+1/+2) = 1.26$ V, while the one electron oxidation processes of compounds **1**, **3** and **5** are chemically quasi-reversible, and become chemically reversible only at high scan rates ($\geqslant 5$ V/s). The other derivatives show either a chemically irreversible oxidation or none at all. It is interesting to note that the substitution of Cl^- by pyridine results in a reversible Re(I)/Re(II) oxidation, the latter being usually chemically irreversible at low scan rates [24]. This could improve the electrogenerated chemiluminescence properties (vide infra) and can be attributed to the better donor properties of pyridine relative to chloride which stabilizes the higher oxidation state.

The half-wave redox potentials, evaluated as a mean of the cyclic voltammetric anodic and cathodic peaks, are reported in Table 4. As can be seen, the compounds containing an N atom in the benzo-X-azole ring (**1**, **4**, **7**, **10**) show more negative reduction potentials compared with the corresponding oxygen and sulfur containing compounds. For instance in the case of **7**, the process centerd at $E^{\circ}(+1/0) = -1.67$ V is shifted towards more negative values, by about 0.3 V, compared with the corresponding values for **8** and **9**. This is in line with the better σ-donor electronic properties of the ligands containing nitrogen. Similarly, the oxidation potentials for the complexes containing a nitrogen atom benzo-X-azole ring are shifted to less positive potentials reflecting the greater electron density at the metal atom.

2.3. Electronic absorption studies

The electronic absorption spectra of all the prepared complexes were measured at room temperature in acetonitrile solution. Results are summarized in Table 5. Molar extinction coefficients (ε) were evaluated from Lambert–Beer's law plots using five solutions with different dilutions. Absorption bands were assigned on the basis of the documented optical transitions of similar Re(I) complexes [28] and using the singlet excited-states computed as described in Section 4.

Complexes of the type $Re(N–N)(CO)_3L$ contain a reducing metal center and an acceptor ligand with low-energy π^* orbitals. Consequently, these compounds display long-wavelength charge transfer ^{1}MLCT ($d\pi(Re)$-$\pi^*(N–N)$) absorptions in their electronic spectra [1].

The lowest energy transitions of the complexes (350–400 nm) were assigned as a metal-to-ligand charge transfer (^{1}MLCT). The overall view of the experimental UV–Vis absorptions is discussed in Section 2.6.

2.4. Emission properties

The $Re(N–N)(CO)_3L$ compounds have attracted interest because of their excited-state properties. Many of them show an emission in solution, which originates either from a ^{3}MLCT or a ^{3}MLLCT lowest-lying triplet excited state.

The room temperature emission spectra of complexes **7**–**12** compared to $[Ru(bpy)_3]^{2+}$ are shown in Fig. 3a and b. Upon irradiation, complexes **7**–**12** displayed intense emissions located at higher energy than that observed for

Table 4
Half wave potentials (V vs. Fc/Fc^+) for complexes **1**–**12**, calculated as $E^{\circ} \approx E_{1/2} = (E_p^a + E_p^c)/2$, at scan rate of 0.1 V/s in acetonitrile at GC electrode

Complex	$E^{\circ}(0/-1)$	$E^{\circ}(-1/-2)$	$E^{\circ}(-2/-3)$	$E^{\circ}(-3/-4)$	$E^{\circ}(0/+1)$
1	−1.83	−2.27 (irr)	–	–	0.88[a]
2	−1.56	−2.13 (irr)	−2.51 (irr)	–	1.03 (irr)
3	−1.50	−2.24 (irr)	−2.43 (irr)	–	1.01[a]
4	−1.61	−1.97 (irr)	–	–	–
5	−1.33	−1.82 (irr)	−2.38 (irr)	–	1.07[a]
6	−1.26	−1.74 (irr)	−1.97	−2.37	1.06 (irr)
	$E^{\circ}(+1/0)$	$E^{\circ}(0/-1)$	$E^{\circ}(-1/-2)$	$E^{\circ}(-2/-3)$	$E^{\circ}(+1/+2)$
7	−1.67	−2.08 (irr)	–	–	1.26
8	−1.38	−1.87 (irr)	–	–	1.47 (irr)
9	−1.30	−1.76 (irr)	−2.42 (irr)	–	1.41 (irr)
10	−1.37	−1.94 (irr)	–	–	–
11	−1.15	−1.67 (irr)	−2.01	−2.37	1.49 (irr)
12	−1.07	−1.60 (irr)	−1.97	−2.37	–

In the case of chemical irreversible processes (irr), anodic (oxidations) and cathodic (reductions) peak potentials are reported.
[a] Chemically quasi-reversible at a scan rate of 0.1 V/s; E° are evaluated at a scan rate of 5 V/s.

Table 5
Experimental absorptions (E_{abs}) and calculated (E_{calc}) excited state energies, $\times 10^3$ cm^{-1} (nm), molar absorptivities (ε, $\times 10^3$ M^{-1} cm^{-1}), oscillator strength (f), occupied (ψ_o) and virtual (ψ_v) orbitals defining the transition (transition coefficient given in parenthesis), and the corresponding assignment and type of the transition for complexes **1**–**12** in acetonitrile

	E_{abs}		ε	E_{calc}		f	$\psi_o \rightarrow \psi_v$	Assignment	Type
1	26.7	(374) sh	4.07	25.4	(393)	0.08	H-1 → LUMO (0.9)	MLCT	Re,CO,Cl → mpbN
	30.0	(333)	18.6	30.3	(330)	0.35	H-2 → LUMO (0.6)	MLLCT	Re,mpbN → mpbN
	31.2	(320)	18.6	30.8	(325)	0.11	H-4 → LUMO (0.8)	MLLCT	Re,Cl,mpbN → mpbN
				38.2	(262)	0.09	H-2 → L + 2 (0.5)	MLLCT	Re,Cl,mpbN → mpbN
2	26.3	(380) sh	3.03	24.4	(410)	0.07	H-1 → LUMO (0.9)	MLCT	Re,CO,Cl → mpbO
	30.5	(328)	13.5	30.5	(328)	0.43	H-3 → LUMO (0.8)	LC	mpbO → mpbO
	31.7	(315)	16.8	32.3	(310)	0.05	H-4 → LUMO (0.9)	LC	mpbO → mpbO
	33.3	(300)	14.6	32.8	(305)	0.05	HOMO → L + 1 (0.8)	MLCT	Re,Cl → mpbO
3	25.3	(395) sh	3.20	23.6	(424)	0.08	H-1 → LUMO (0.9)	MLCT	Re,CO,Cl → mpbS
	29.2	(343)	14.5	29.4	(340)	0.06	H-4 → LUMO (0.9)	LC	mpbS → mpbS
	30.5	(328)	15.1	29.8	(336)	0.42	H-3 → LUMO (0.8)	LC	mpbS → mpbS
	33.3	(300)	10.3	34.5	(290)	0.06	HOMO → L + 3 (0.3)	MLCT	Re,Cl → mpbS
4	24.4	(410) sh	4.93	23.5	(426)	0.07	H-1 → LUMO (0.9)	MLCT	Re,CO,Cl → mqbN
	27.5	(363)	26.4	27.5	(363)	0.43	H-2 → LUMO (0.7)	MLLCT	Re,mqbN → mqbN
				29.1	(344)	0.09	H-5 → LUMO (0.9)	LC	mqbN → mqbN
	33.7	(297)	21.6	33.7	(297)	0.05	H-1 → L + 1 (0.6)	MLCT	Re,Cl → mqbN
5	25.0	(400) sh	4.19	22.9	(436)	0.08	H-1 → LUMO (0.9)	MLCT	Re,CO,Cl → mqbO
	28.0	(357)	18.9	27.5	(364)	0.21	H-2 → LUMO (0.7)	MLLCT	Re,mqbO → mqbO
	29.2	(343)	18.3	28.2	(354)	0.37	H-4 → LUMO (0.8)	LC	mqbO → mqbO
	33.9	(295)	16.2	33.3	(304)	0.05	HOMO → L + 2 (0.6)	MLCT	Re,Cl → mqbO
6	24.1	(415) sh	3.56	22.4	(446)	0.08	H-1 → LUMO (0.9)	MLCT	Re,CO,Cl → mqbS
	26.9	(372)	21.7	27.0	(371)	0.19	H-2 → LUMO (0.6)	MLLCT	Re,mqbS → mqbS
	28.2	(354)	19.0	27.7	(361)	0.40	H-4 → LUMO (0.7)	LC	mqbS → mqbS
	33.6	(298)	12.7	32.3	(310)	0.05	HOMO → L + 1 (0.9)	MLCT	Re,CO,Cl → mqbS
7	27.3	(366) sh	5.95	26.9	(372)	0.09	H-1 → LUMO (0.8)	MLCT	Re,CO → mpbN
	30.3	(330)	20.6	30.0	(333)	0.44	H-2 → LUMO (0.8)	MLLCT	Re,mpbN → mpbN
				33.3	(300)	0.06	H-1 → L + 1 (0.6)	MLCT	Re,CO → py
	35.5	(282)	12.8	35.6	(281)	0.06	H-1 → L + 42 (0.4)	MLCT	Re,CO → py,mpbN
8	27.0	(370) sh	4.58	26.4	(379)	0.08	H-1 → LUMO (0.7)	MLCT	Re,CO → mpbO
	30.5	(328)	15.3	30.4	(328)	0.46	H-3 → LUMO (0.8)	MLLCT	Re,mpbO → mpbO
	31.7	(315)	16.5	33.7	(300)	0.05	H-1 → L + 1 (0.5)	MLCT	Re,CO → py
				33.9	(295)	0.06	HOMO → L + 2 (0.8)	MLCT	Re,CO → mpbO
				35.8	(280)	0.08	H-1 → L + 2 (0.6)	MLCT	Re,CO → py,mpbO
9	26.3	(380) sh	4.74	25.7	(389)	0.09	H-1 → LUMO (0.8)	MLCT	Re,CO → mpbS
	29.2	(343)	15.8	29.1	(344)	0.20	H-3 → LUMO (0.6)	MLLCT	Re,mpbS → mpbS
	29.9	(334)	15.4	29.8	(336)	0.26	H-4 → LUMO (0.7)	MLLCT	Re,mpbS → mpbS
				33.0	(303)	0.06	HOMO → L + 1 (0.7)	MLCT	Re,CO → py
				33.7	(297)	0.05	HOMO → L + 2 (0.7)	MLCT	Re,CO → mpbS
	35.3	(283)	10.1	35.6	(281)	0.07	H-1 → L + 2 (0.5)	MLCT	Re,CO → py,mpbS
10	24.4	(410) sh	4.47	25.0	(400)	0.09	H-1 → LUMO (0.8)	MLCT	Re,CO → mqbN
	27.5	(363)	22.0	27.4	(365)	0.51	H-2 → LUMO (0.8)	MLLCT	Re,mqbN → mqbN
				31.8	(314)	0.05	HOMO → L + 1 (0.8)	MLLCT	Re,mqbN → py
	33.4	(299)	18.7	33.7	(297)	0.11	HOMO → L + 2 (0.7)	MLLCT	Re,CO,mqbN → mqbN
				34.5	(290)	0.05	H-7 → LUMO (0.4)	MLCT	Re → mqbN
							H-1 → L + 2 (0.4)		
11	27.5	(380) sh	5.94	24.7	(405)	0.10	H-1 → LUMO (0.8)	MLCT	Re,CO → mqbO
				27.4	(365)	0.23	H-2 → LUMO (0.6)	MLLCT	Re,mqbO → mqbO
	29.1	(344)	13.6	28.3	(353)	0.35	H-4 → LUMO (0.7)	MLLCT	Re,mqbO → mqbO
	33.8	(298)	14.2	32.9	(304)	0.07	HOMO → L + 1 (0.7)	MLCT	Re → py
				34.2	(292)	0.07	H-7 → LUMO (0.5)	MLLCT	Re,mqbO → mqbO
				37.0	(270)	0.12	H-1 → L + 2 (0.4)	MLCT	Re,CO → py,mqbO

Table 5 (*continued*)

	E_{abs}		ε	E_{calc}		f	$\psi_o \rightarrow \psi_v$	Assignment	Type
12	24.7	(405) sh	4.46	24.1	(415)	0.08	H-1 → LUMO (0.8)	MLCT	Re,CO → mqbS
	26.1	(373)	15.1	27.0	(370)	0.53	H-2 → LUMO (0.8)	MLLCT	Re,mqbS → mqbS
	27.8	(360)	13.9	28.6	(350)	0.06	H-5 → LUMO (0.9)	MLLCT	Re,CO,mqbS → mqbS
	33.2	(301)	10.7	32.7	(306)	0.09	HOMO → L + 1 (0.6)	MLCT	Re,CO → py,mqbS
				33.7	(297)	0.10	HOMO → L + 2 (0.4)	MLCT	Re → py,mqbS
				35.7	(280)	0.07	H-1 → L + 2 (0.3)	MLCT	Re → py,mqbS

$[Ru(bpy)_3]^{2+}$. Complexes **1**–**6** are only weakly emissive (**1**–**4**) or non-emissive (**5**, **6**) at RT. Photophysical data are shown in Table 6. It is noteworthy that Φ_{em} of **7** (0.075) is higher than the corresponding value of $[Ru(bpy)_3]^{2+}$ (0.065), but is about half the value of the analogous bipyridyl complex $[Re(bpy)(CO)_3(py)]^+$ (0.16) [27].

Since imidazoles are only weak electron acceptors, the MLCT luminescence of $Re(N–N)(CO)_3Cl$ complexes which contain diimines with imidazole subunits appear at rather short wavelengths [29].

There are also many Re(I) carbonyl complexes with lowest-energy MLCT states which are non-emitting because the MLCT states are deactivated by radiationless decay to the ground-state. This situation applies to complexes with MLCT states at rather low energies and the lack of emission may be attributed to the energy gap law [27].

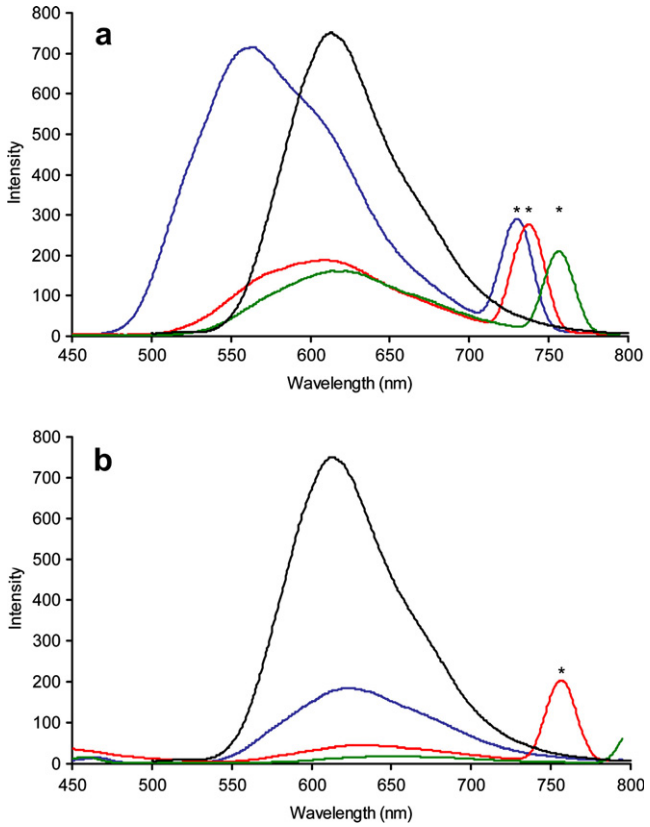

Fig. 3. Room temperature emission spectra of complexes: (a) **7** (blue), **8** (red), **9** (green) compared to $[Ru(bpy)_3]^{2+}$ (black). (b) **10** (blue), **11** (red), **12** (green) compared to $[Ru(bpy)_3]^{2+}$ (black); (peaks marked with * are harmonic leakage from excitation radiation). (For interpretation of the references to colour in this figure legend, the reader is referred to the web version of this article.)

In general, excited-states of rhenium complexes of formula $Re(N–N)(CO)_3L$ depend on the trade off between ^{3}MLCT states and ^{3}LC states. The energy of these states and their relative position to each other is related to the nature of the diimine ligand, N–N, and to the nature of the ancillary ligand L. For example, when L can be easily oxidizes, ^{3}LLCT states become the lowest-lying [30]. The presence of low energy ^{3}d–d states is also important, because it affects the emission process by allowing radiationless decay pathways [28]. Nevertheless, the character of the orbitals involved in the electronic transitions and the exact nature of the excited-states are poorly defined in many cases. TDDFT calculations can be a powerful tool for helping in the assignment of these states.

2.5. ECL measurements of complexes 7–9

The redox and ECL properties of similar compounds have been reported previously by Kapturkiewicz et al. [26]. The difference between the potentials of the first oxidation and the first reduction for complexes **7**–**9** are equal or greater than 2.7 V, a considerably higher value than the energy relative to the ^{3}MLCT luminescence. The oxidized and reduced forms of the rhenium complexes under investigation were generated using a multicycle double potential step technique, alternating the oxidation and reduction potentials, in order to generate a train of closely spaced light pulses. The potential step intervals were set to 1s. With this period, the compound **7** reaches a steady-state ECL response, indicating that both the oxidized and reduced forms are chemically stable. On the contrary, com-

Table 6
Photoemission data in $\times 10^3$ cm^{-1} (and nm) for complexes **1**–**12** in acetonitrile

	Excitation	Emission	ϕ_{em}
$[Ru(bpy)_3]^{2+}$	22.2 (450)	16.3 (614)	0.062
1	26.7 (374)	16.4 (610)	0.009
2	26.3 (380)	15.7 (635)	0.002
3	25.3 (395)	15.6 (640)	0.001
4	24.4 (410)	15.6 (641)	0.001
5	25.0 (400)	–	–
6	24.1 (415)	–	–
7	27.3 (366)	17.7 (565)	0.075
8	27.0 (370)	16.4 (610)	0.020
9	26.3 (380)	16.1 (620)	0.016
10	24.4 (410)	16.0 (625)	0.022
11	25.7 (380)	15.7 (635)	0.005
12	24.7 (405)	15.2 (660)	0.003

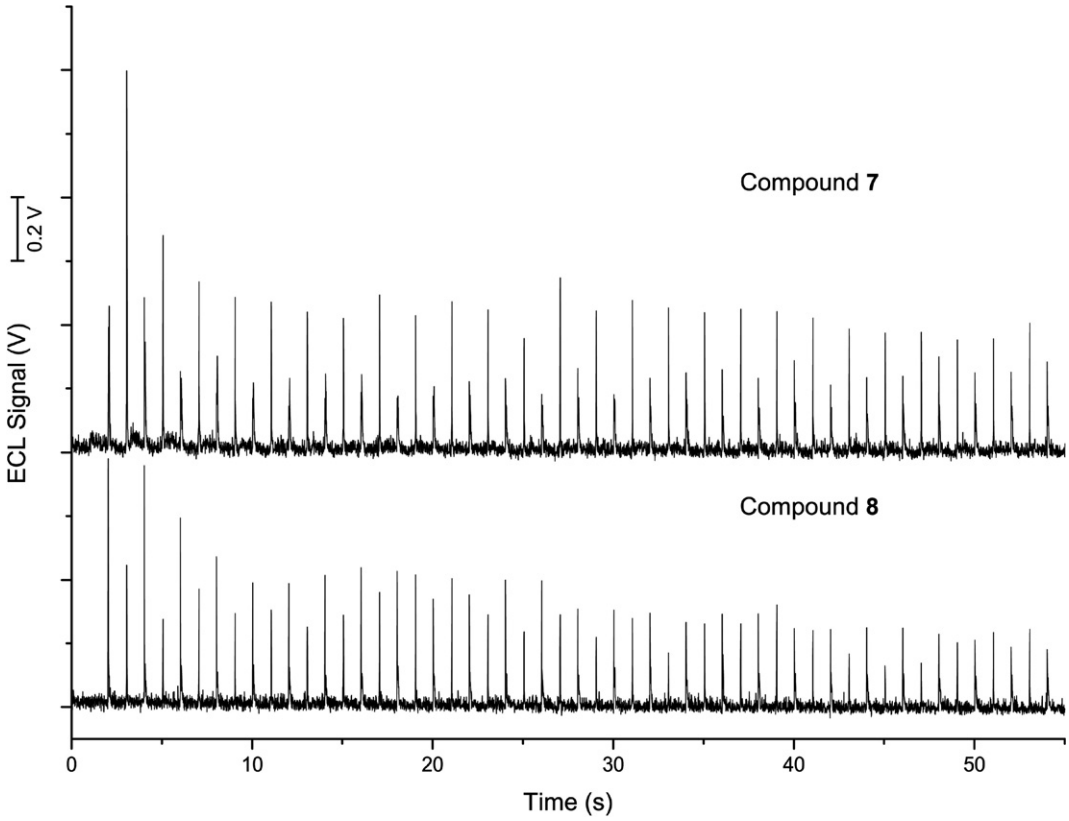

Fig. 4. ECL responses by applying a multicycle double potential step to a 3.2×10^{-5} M acetonitrile solutions of **7** and **8**.

pounds **8** and **9** show ECL signals that do not reach steady-state ECL responses. This is easily explained considering that the oxidations observed for **8** and **9** are chemically irreversible. Fig. 4 compares the ECL responses of **7** and **8**. The first potential steps for each compound were used to evaluate the corresponding ECL efficiencies ϕ_{ecl} (in numbers of emitted photons per number of annihilating pairs) [31] using $[Ru(bpy)_3]^{2+}$ as standard with $\phi^{\circ}_{ecl} = 0.05$ [32]. ϕ_{ecl} for compounds **7**, **8** and **9** were evaluated to be 0.005, 0.003 and 0.001, respectively. These values fit well with those previously reported for similar compounds [26], and are in agreement with the observed emission quantum yields ϕ_{em} (see Table 5).

2.6. Computational studies

The gas phase geometries of compounds **1**–**12** were fully optimized in the singlet ground-state using the B3LYP [33,34] functional of GAUSSIAN-03 [35]. The Stuttgart–Dresden (SDD) ECP [36] was chosen for rhenium atoms and the 6-31G(d,p) basis set was employed for all other atoms. The ground-state gas phase structures of **7**–**9** were reoptimized in acetonitrile as solvent, using the PCM calculation available in GAUSSIAN-03. The geometries of the lowest-lying triplet states, taken as models of the corresponding emitting states [37], were determined with the unrestricted B3LYP method in the gas phase. The nature of all stationary points was confirmed by performing a normal mode analysis.

TDDFT/PCM [38–40] calculations were employed to produce a number (32) of singlet excited-states starting from the ground-state geometry optimized in the gas phase. The assignments of the transition states are based on the major contributing excitation (i.e. when the transition coefficient of the major excitation is higher than that of the other excitations by more than 0.2). Mixed singlet excited-states where the differences among the major excitation and the others excitation is less than 0.2 were not found for the studied molecules. TDDFT does not provide the electronic structures of the excited states, however, the electronic distribution and the localization of the excited states may be visualized using the electron density difference maps (EDDMs) [37]. With this method we take in account for all the contributing excitations. The EDDMs for all compounds were calculated and employed for the correct assignments of the transitions type. The GAUSSSUM program [41] was used for EDDMs, for the representation of the absorption spectra and for analysing the contribution of different groups of atoms to MOs. This approach has precedent in the literature for determining the excited-state structures and electron distributions associated with metal complexes containing diimine and π-acceptor ligands [28,42,43].

2.6.1. Molecular orbitals of complexes 7–9

The molecular orbital diagram for complexes **7**–**9** is depicted in Fig. 5. Re_d contribution to the HOMO orbital is 38, 49 and 50% for **7**, **8** and **9**, respectively. A consider-

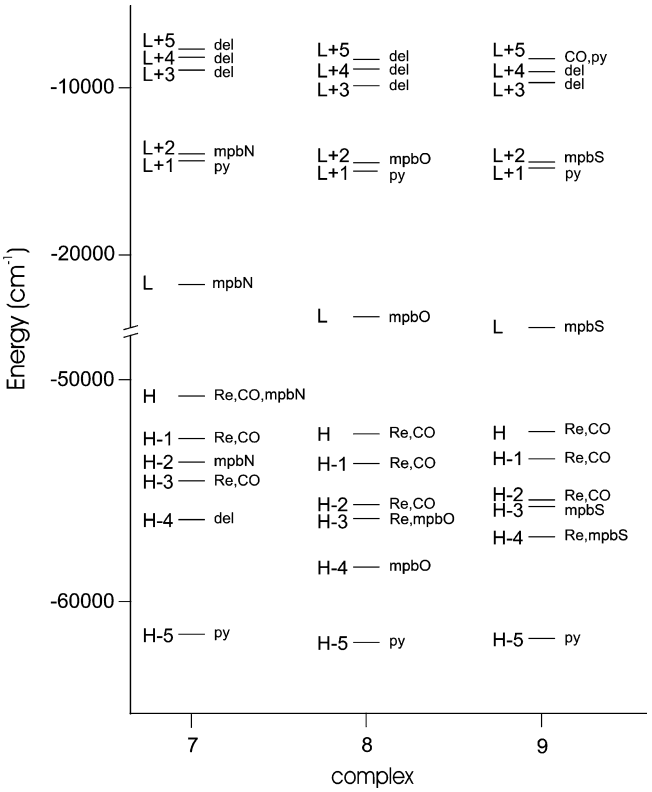

Fig. 5. Molecular orbital energy diagram for six occupied and six virtual frontiers orbitals of **7**–**9** in the singlet ground-state in acetonitrile.

able contribution is coming from the CO orbitals (17% for **7** and 21% for both **8** and **9**) and also from π^*-diimine orbitals, especially for complex **7**. In fact, **7** has 42% of the HOMO localized on the mpbX ligand, while it is 26 and 24% for **8** and **9**, respectively (Fig. 6).

Higher Re_d character is present in the H-1 (52%) and H-3 (67%) orbitals of **7**, in the H-1 (56%) and H-2 (67%) orbitals of **8** and in the H-1 (50%) and H-2 (61%) orbitals of **9**. All these orbitals have a relatively considerable CO character, ranging from 20% to 29%. In the three metal-complexes there is a 99% pyridine-centerd orbital (H-5).

The LUMO π^*-diimine character is higher than 93% in all complexes. L + 2 orbitals have a high π^*-mpbX character, L + 1 molecular orbitals are mainly centered on the pyridine ligand, while the highest virtual orbitals are delocalized among Re, carbonyls and pyridine (about 90%). The HOMO–LUMO energy gap decreases passing from **7** to **9**: 30.7×10^3 (**7**), 30.5×10^3 (**8**), and 29.7×10^3 cm^{-1} (**9**).

2.6.2. Geometry optimization of the lowest-lying triplet excited states of 7–9

Lowest-lying triplet-state geometries were computed in the gas phase starting from the optimized structure in the ground-state. Unrestricted B3LYP was utilized. The spin contamination from states of higher multiplicity was low. The $\langle S^2 \rangle$ values were 2.020 (**7**), 2.026 (**8**) and 2.027 (**9**). Significant structural changes occur between the geometries of

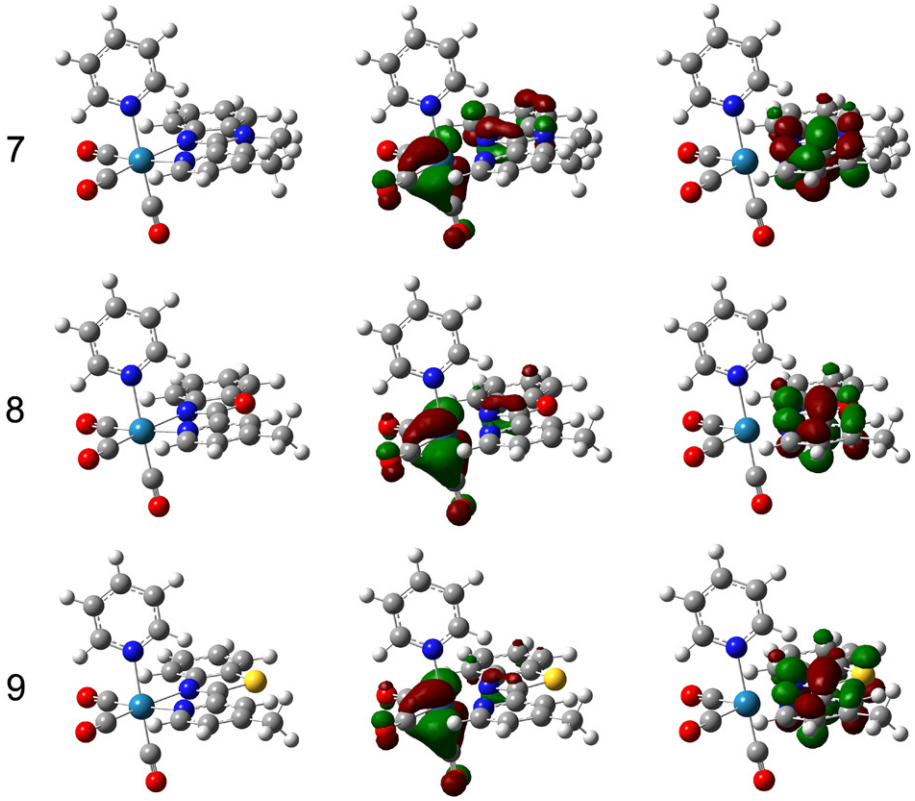

Fig. 6. HOMO (middle) and LUMO (right) orbital representations for complexes **7**–**9** in the singlet ground-state in acetonitrile.

Table 7
Bond lengths (Å) and angles (°) calculated at the B3LYP level for the ground and lowest ^{3}MLCT excited states of complexes **7**–**9**

	7		**8**		**9**	
	Ground	^{3}MLCT	Ground	^{3}MLCT	Ground	^{3}MLCT
Re–C1	1.95	1.97	1.95	1.97	1.95	1.98
Re–C2	1.94	1.95	1.94	1.95	1.94	1.94
Re–C3	1.94	1.99	1.94	1.99	1.94	1.98
Re–N1	2.24	2.20	2.26	2.20	2.23	2.20
Re–N2	2.20	2.11	2.22	2.11	2.24	2.14
Re–N4	2.28	2.27	2.28	2.27	2.28	2.26
C1–Re–C2	90.43	91.30	90.49	91.29	90.48	90.97
C1–Re–C3	90.58	89.96	90.12	90.15	90.52	90.38
C2–Re–C3	90.41	89.76	91.24	90.33	89.60	88.77

the ground-states and the geometries of the lowest-lying triplet excited-states of **7**–**9**, namely the ^{3}MLCT states. The calculations provide a good description of bond distances and angles, and furthermore illustrate the changes in such parameters on going from the ground-state to the lowest-lying triplet state. Selected bond distances and angles are reported in Table 7. In the optimized ground-state structure the HOMO has a significant Re_d–π^*(CO) character (from 55% to 70%). Ligand contributions are also important and localized totally on the benzo-X-azole side of the ligand. The LUMO is mainly centered on the mpbX ligand (>93%) (see Fig. 7a and b). The TDDFT calculations (see below) show that the MLCT transitions occur from H-1 to LUMO of the ground state (Fig. 7b). This is nearly unchanged with respect the single-occupied HOMO of the triplet emitting state (Fig. 7d). Therefore, the lowest-lying triplet state closely corresponds to this excitation, and its geometry can be a reasonable approximation of the real emitting state. Significant orbital relaxation occurs in the H-1 compared to HOMO in the triplet excited and ground states, respectively (Fig. 7c and a).

In compound **7**, the Re–C(1) and Re–C(3) bond elongations of 0.02 Å and 0.05 Å observed in the ^{3}MLCT state, can be explained by taking into account the greater bonding nature of the HOMO orbital in the ground-state, which is depopulated in the ^{3}MLCT state. This bonding character was determined by visual examination of the phase of the different molecular orbitals [44]. Similar considerations can be applied to complexes **8** and **9**.

Other structural changes due to the MLCT transition can be explained by looking at the two natural orbitals which contain the unpaired spins (H-1 and HOMO), Fig. 7c and d. The orbital H-1 has a reduced Re_d–π^*(CO) character, in fact there is a consistent migration of electronic amplitude onto the Me-pyridine ring of the mpbN ligand. This mixing between the HOMO and LUMO orbitals accounts for the Re–N(2) (0.11 Å for **8**) and Re–N(1) (0.06 Å for **8**) distance shortening, as reported in Table 7 [45]. Partial oxidation of the metal center gives a reduction in CO back-bonding and thus a related increase in the σ-bond interaction with the nitrogen-ligands.

The DFT calculation predicts a decrease in the equatorial CO–Re–CO angle in the triplet excited-state. This is consistent with the higher antibonding nature of the π^*(mpbX)–π^*(CO) orbital overlap. A general trend for the axial–equatorial carbonyl angles is less straightforward and is not described in detail.

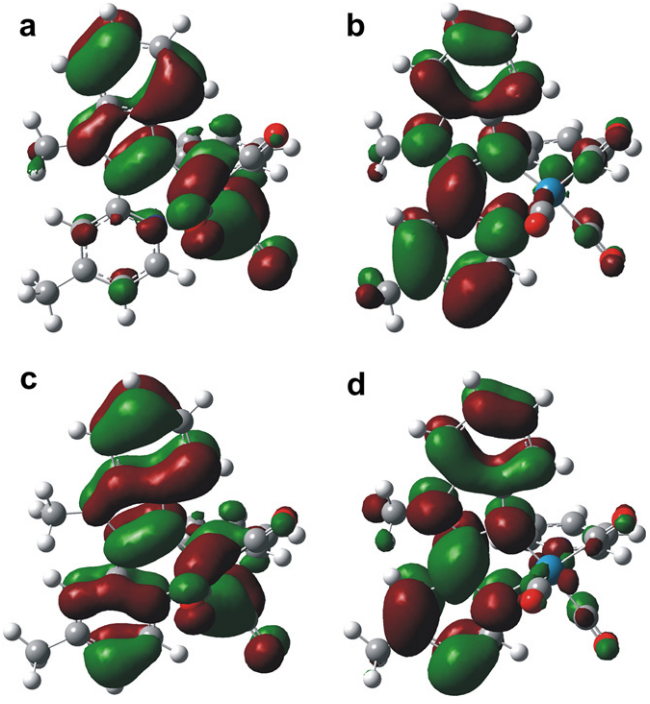

Fig. 7. HOMO (a) and LUMO (b) orbitals for complex **7** in the singlet ground-state and single occupied H-1 (c) and HOMO (d) orbitals for the lowest-lying triplet state of the same complex.

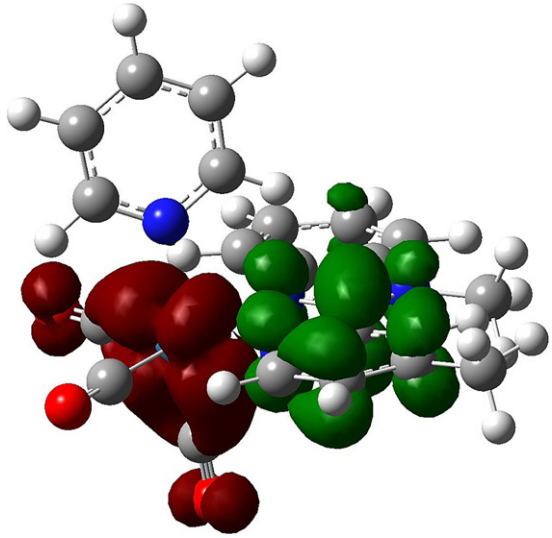

Fig. 8. Electron density difference map (EDDM) of the lowest energy singlet electronic transition of **7** (MLCT). Red indicates a decrease in charge transfer, while green indicates an increase. (For interpretation of the references to colour in this figure legend, the reader is referred to the web version of this article.)

*2.6.3. Calculated absorption spectra and emission energies of **1–12***

The calculated TDDFT transitions are generally in good agreement with the experimental absorptions (Table 5). The nature of the transitions calculated by TDDFT that characterize the absorption spectra may be visualized using the electron density difference maps (EDDMs). For instance, the EDDM of the MLCT transition at 26900 cm^{-1} of complex **7** (Fig. 8) clearly shows a decrease in charge density at the metal center (in red), and a corresponding increase on the mpbN ligand (in green).[1] This approach greatly simplifies the assignment process. The calculated and experimental absorption spectra for complexes **7–9** are reported in Fig. 9. The bars represent the computed transition with height equal to the corresponding oscillator strengths (f). Only transitions with $f > 0.05$ are shown in Table 5. The singlet excited-states with lower energy are of MLCT type for all complexes. These transitions occur from the orbital H-1, which is mainly centered on the metal, to the LUMO, which is almost completely centered on the ligand mpbX or mqbX.

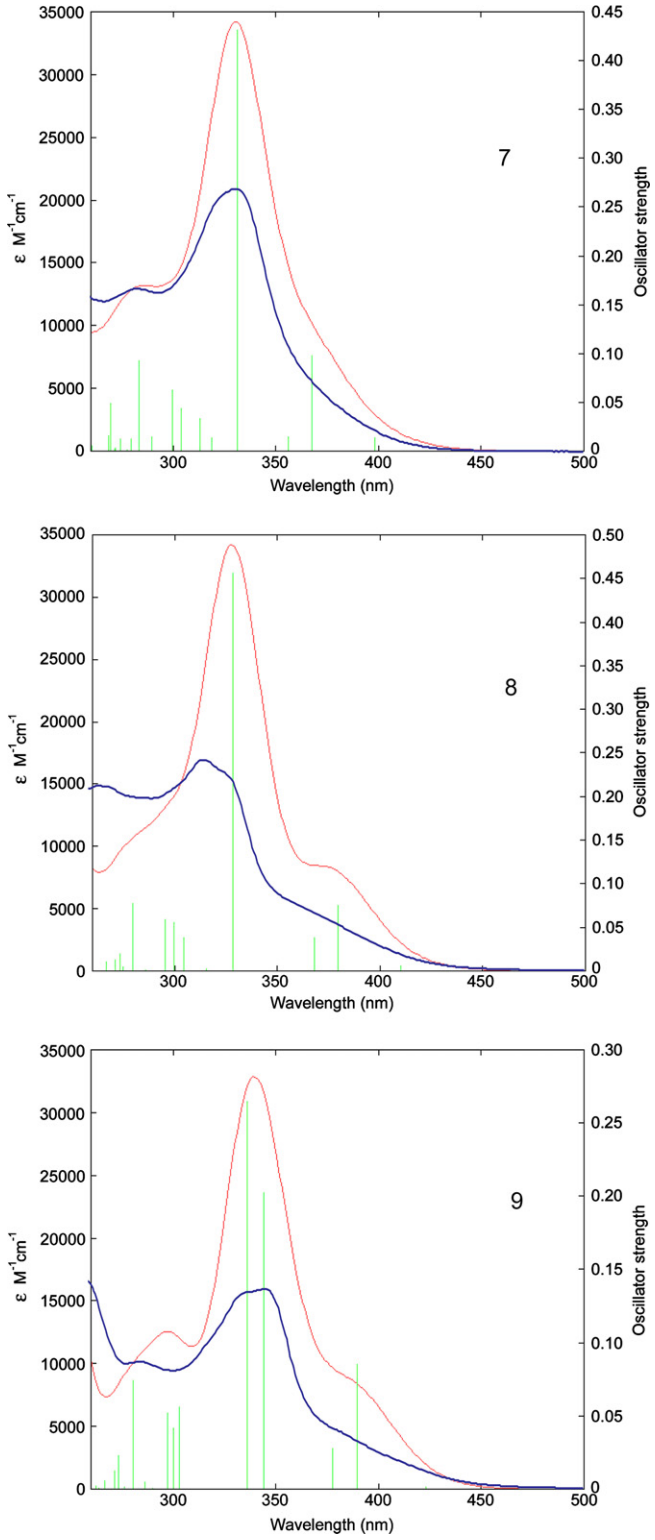

Fig. 9. Calculated and experimental absorption spectra for complexes **7–9**. Curves were obtained using the program GAUSSSUM 1.0.

The absorptions with the highest ε are generally MLLCT transition, with the exception of **2** (LC), **3** (LC), **5** (MLLCT and LC) and **6** (MLLCT and LC). Noteworthy, these are the complexes with the lowest ϕ_{em} (Table 6), and do not contain nitrogen in mpbX or mqbX. It is interesting to note also that the introduction of pyridine in compounds **7–12** has the effect to mix the metal- with the ligand-centered orbitals involved in the excited state transitions, resulting into the shift of the pure LC transitions at higher energies.

The emission energy were evaluated employing the ΔSCF (self-consistent field) approach, i.e. considering the vertical energy gap between the S_0 and T_1 energies, both evaluated at the optimized geometry of T_1 [37]. The experimental trend of the emission energies (17700, 16400 and 16100 cm^{-1}) is well reproduced by the calculation (16000, 15000 and 14900 cm^{-1}, for **7**, **8** and **9**, respectively).

3. Conclusions

In summary these investigations reveal that the nitrogen containing bicyclic heterocycle in **7** provides electrochemical and photophysical properties that have the best potential for use as biosensors and as probes for studying biomolecular structure and dynamics. This was also the case for the previously reported $Ru(bpy)_2(mpbX)^{2+}$ complexes (X = N, O, S) [15]. The TDDFT calculations provide insight into the reasons why **7** shows reversible redox behaviour, higher quantum yield and longer excited state lifetime than the other complexes based on the calculated energy gaps and the orbital contributions to the ground and excited states. Ground and excited-state calculations enable a detailed assignment to be made of the electronic absorption and emission spectra of the tricarbonylrhenium derivatives. TD-DFT applied to organometallic compounds resulted in appropriate prediction

[1] For interpretation of the references to colour in Fig. 8, the reader is referred to the web version of this article.

of the UV–Vis spectra. The shape of LUMOs in the ground state and the shape of HOMOs in the lowest-lying triplet excited-states are similar, suggesting that the calculated lowest-lying triplet excited-states are a reasonable approximation of the real emitting states. In fact, the calculated emission energies are in good agreement with the experimental values. The reversible redox processes observed for complex **7**, pointed out the better ϕ_{ecl} values with respect the other complexes.

4. Experimental

4.1. Materials and reagents

All solvents in the synthetic procedures were of analytical reagent grade and purified according to the literature procedures [46]. $Re(CO)_5Cl$, $AgNO_3$, NH_4PF_6, pyridine and tetrabutylammonium trifluoromethanesulfonate (TBAOTf) were purchased from Aldrich and used as received without further purification. Tetrabutylammonium hexafluorophosphate ($TBAPF_6$) was obtained by a metathesis reaction between KPF_6 (Fluka) and tetrabutylammonium iodide (Aldrich), re-crystallized three times from 95% ethanol and dried in vacuum oven at 110 °C overnight.

4.2. Physical methods

NMR spectra were recorded on a JEOL EX 400 spectrometer ($B_0 = 9.4$ T, ^1H operating frequency 399.78 MHz) with chemical shifts referenced to residual protons in the solvent. Infrared spectra were obtained as KBr pellets, using a Bruker Equinox 55 FT-IR spectrophotometer, with a resolution of 1 cm^{-1} and an accumulation of 64 scans. Electronic absorption spectra were measured in CH_3CN, using a double-beam Perkin–Elmer Lambda 20 UV–visible spectrophotometer equipped with 1-cm quartz cell. Steady-state luminescence measurements were performed with a Perkin–Elmer LS 55 spectrofluorimeter and 1-cm fluorescence cell, using deoxygenated acetonitrile solutions with absorbance of about 0.10 at the lowest energy transition, in order to exclude self-quenching processes. Quantum yields were calibrated using $[Ru(bpy)_3]^{2+}$ in deoxygenated acetonitrile. All spectrophotometric measurements were carried out at room temperature. Electrochemistry was performed both with an EG & G PAR 273 electrochemical analyzer and an AMEL 7050 potentiostat connected to a PC. All experiment employed a standard three-electrode electrochemical cell: a Glassy Carbon Electrode (GCE, $\varnothing = 3$ mm) as a working electrode, a Pt wire as a counter, and a calomelane (KCl 3 M) as reference electrode were used. Positive feedback iR compensation was applied routinely. All measurements were carried out under Ar in anhydrous deoxigenated solvents. We used ferrocene (Fc) as internal standard, and potentials are reported against the Fc(0/+1) redox couple (measured $E_{1/2}(0/+1) = 0.372$ V in CH_3CN). The ECL along with CV signals were measured with the AMEL 7050. The home-build instrumentation has been described elsewhere [15]. Mass spectra were recorded using either direct inlet probe or electron spray ionization. Direct inlet probe analyses were performed with a Thermo Finnigan Trace MS Plus. The samples were dissolved in acetonitrile. Ionization occurred by EI mode with electron energy at 70 eV. Electron spray mass analyses were performed with a Thermo Finnigan LCQ Advantage Max equipped with an ion trap analyzer. The samples, dissolved in a methanol/acetonitrile/water acidified with TFA (0.1%) mix, were recorded in ions positive mode. The comparisons of the experimental and simulated isotopic pattern were excellent.

4.3. DFT calculations

Density functional calculations were carried out with GAUSSIAN-03 [35] program. The singlet ground-state geometries of the complexes **1**–**12** were optimized in the gas phase by the B3LYP [33,34] functional. The Stuttgart–Dresden (SDD) ECP [36] was employed for the Re atom and the 6-31G(d,p) basis set for all other atoms. Time-dependent density functional theory [47,48] (TD DFT) combined with the polarizable continuum model (PCM) method with acetonitrile as solvent has been used to calculate the excited-state energies by means of G03. The nature of all stationary points was confirmed by performing the normal mode analysis. Other details on the calculation method are described previously in Section 2.5.

4.4. X-ray structure determinations

Single crystal diffraction data were collected on a Oxford Xcalibur CCD area detector diffractometer, using graphite monochromatic Mo Kα ($\lambda = 0.71069$Å) radiation. Data reduction and absorption correction were performed using CrysAlis RED 1.171.26 (Oxford Diffraction). The structure was solved by direct methods using SIR-2002 [49] and refined by full-matrix least-squares using SHELX-97 [50]. Hydrogen atoms were generated in calculated position using SHELX-97. For compound **1** it was not possible to find an high quality crystal and the data collection was limited to $\theta < 23.24°$ (corresponding to resolution >0.90 Å). However, a reliable crystal structure with acceptable e.s.d.'s was obtained.

Details of data collections and refinements are given in Table 1.

4.5. Synthesis of the ligands

The ligands 2-(4-methylpyridin-2-yl)benzo[*d*]-X-azole, with X = N–CH_3 (mpbN), O (mpbO), and S (mpbS), and the 2-(benzo[*d*]-X-azol-2-yl)-4-methylquinoline, with X = O (mqbO), and S (mqbS) were prepared according to published procedures [51,52].

4.5.1. Synthesis of [4-methyl-2-(1-methyl-1H-benzo[d]imidazol-2-yl)quinoline] (mqbN)

Reaction of 2-(1*H*-benzo[*d*]imidazol-2-yl)-4-methylquinoline (1.0 g, 3.86×10^{-3} mol) with methyl iodide (2.03 g, 1.43×10^{-2} mol) and potassium *tert*-butoxide (0.56 g, 4.99×10^{-3} mol) using 15 mL of diethyl ether and 6 mL of *N*,*N*-dimethylformammide as solvent, at a temperature of 50 °C. After 3 h, the mixture was poured into water and extracted with ethyl ether. The ethyl ether was dried with anhydrous sodium sulfate and evaporated. The crude product was adsorbed onto silica gel and purified by flash chromatography (acetone/petroleum benzene; 5:95). An off-white powder was finally obtained. Yield: 80%. ^{1}H NMR ($CDCl_3$) $\delta = 2.79$ (s, 3H), 4.46 (s, 3H), 7.32–7.39 (m, 2H), 7.48 (d, $^3J_{H,H} = 7.6$, 1H), 7.61 (t, $^3J_{H,H} = 8.3$, 1H), 7.75 (t, $^3J_{H,H} = 7.6$, 1H) 7.89 (d, $^3J_{H,H} = 8.3$, 1H), 8.04 (d, $^3J_{H,H} = 9.0$, 1H), 8.16 (d, $^3J_{H,H} = 8.3$, 1H), 8.41 (s, 1H). ^{13}C NMR (DMSO-d_6) 18.80, 33.21, 110.11, 120.33, 122.36, 122.77, 123.68, 123.97, 127.15, 128.02, 129.57, 130.38, 137.68, 142.76, 145.14, 147.31, 150.33, 150.43. MS (ESI): *m*/*z* 274 $[M+1]^+$.

4.6. General synthesis of fac-Re(N–N)(CO)$_3$Cl

Chloro complexes, Re(N–N)$(CO)_3$Cl, were obtained with a slight modification of a previously published procedure [27]; equimolar quantities of $Re(CO)_5Cl$ were heated at reflux with the appropriate N–N ligand in toluene (N–N = mpbN (**1**), mpbO (**2**), mpbS (**3**), mqbN (**4**), mqbO (**5**), mqbS (**6**)) for 4h. The yellow or orange products were precipitated pure from solution and then filtered and used without further purifications.

4.6.1. fac-Re(mpbN)(CO)$_3$Cl (**1**)

Yield: 59%. Anal. Calc. for $C_{17}H_{13}Cl_1N_3O_3Re_1$ (528.97): C, 38.60; H, 2.48; N, 7.94. Found: C, 38.60; H, 2.49; N, 7.79%. IR (KBr pellets, cm^{-1}): 1900 (s), 1917 (s), 2017 (s). ^{1}H NMR (acetone-d_6): $\delta = 2.68$ (s, 3H), 4.54 (s, 3H), 7.60–7.63 (m, 2H), 7.67 (d, $^3J_{H,H} = 4.9$ Hz, 1H), 7.91–7.93 (m, 1H), 8.60 (s, 1H), 9.05 (d, $^3J_{H,H} = 5.6$ Hz, 1H). ^{13}C NMR (acetone-d_6): $\delta = 21.56$, 33.84, 112.69, 119.58, 126.10, 126.76, 126.80, 128.97, 137.22, 141.01, 147.90, 153.56, 154.73. Electronic spectrum in CH_3CN: absorption, λ_{max} (nm) = 320, 333, 374; emission, λ_{max} (nm) = 610.

4.6.2. fac-Re(mpbO)(CO)$_3$Cl (**2**)

Yield: 63%. Anal. Calc. for $C_{16}H_{10}Cl_1N_2O_4Re_1$ (515.93): C, 37.25; H, 1.95; N, 5.43. Found: C, 36.83; H, 1.89; N, 5.21%. IR (KBr pellets, cm^{-1}): 1898 (s), 1912 (s), 2018 (s). ^{1}H NMR (acetone-d_6): $\delta = 2.73$ (s, 3H), 7.78–7.82 (m, 3H), 7.97–8.05 (m, 2H), 8.45 (s, 1H), 9.04 (d, $^3J_{H,H} = 5.6$ Hz, 1 H). ^{13}C NMR (acetone-d_6): $\delta = 21.38$, 113.38, 119.89, 127.02, 128.51, 129.69, 131.18, 139.41, 144.27, 151.72, 154.38, 154.70. Electronic spectrum in CH_3CN: absorption, λ_{max} (nm) = 300, 315, 328, 380; emission, λ_{max} (nm) = 635.

4.6.3. fac-Re(mpbS)(CO)$_3$Cl (**3**)

Yield: 55%. Anal. Calc. for $C_{16}H_{10}Cl_1N_2O_3Re_1S$ (531.99): C, 36.12; H, 1.89; N, 5.26. Found: C, 35.95; H, 1.76; N, 5.13%. IR (KBr pellets, cm^{-1}): 1902 (s), 1914 (s), 2022 (s). ^{1}H NMR (acetone-d_6): $\delta = 2.67$ (s, 3H), 7.73 (d, $^3J_{H,H} = 5.7$ Hz, 1H), 7.79 (t, $^3J_{H,H} = 7.9$ Hz, 1H), 7.93 (t, $^3J_{H,H} = 7.6$ Hz, 1H), 8.39 (d, $^3J_{H,H} = 8.4$ Hz, 1H), 8.45 (d, $^3J_{H,H} = 8.5$ Hz, 1H), 8.49 (s, 1H), 9.05 (d, $^3J_{H,H} = 5.6$ Hz, 1H). ^{13}C NMR (acetone-d_6): $\delta = 21.27$, 124.00, 124.65, 127.39, 129.28, 129.98, 130.36, 127.39, 134.03, 151.62, 152.11, 153.67, 154.42, 154.48. Electronic spectrum in CH_3CN: absorption, λ_{max} (nm) = 300, 228, 343, 395; emission, λ_{max} (nm) = 640.

4.6.4. fac-Re(mqbN)(CO)$_3$Cl (**4**)

Yield: 88%. Anal. Calc. for $C_{21}H_{15}Cl_1N_3O_3Re_1$ (579.03): C, 43.56; H, 2.61; N, 7.26. Found: C, 43.67; H, 2.47; N, 7.14%. IR (KBr pellets, cm^{-1}): 1891 (s), 1928 (s), 2018 (s). ^{1}H NMR (DMSO-d_6): $\delta = 3.03$ (s, 3H), 4.51 (s, 3H), 7.66–7.68 (m, 2H), 7.94 (t, $^3J_{H,H} = 7.63$ Hz, 1H), 7.98–8.00 (m, 1H), 8.08–8.11 (m, 1H), 8.16 (t, d, $^3J_{H,H} = 8.48$ Hz, $^4J_{H,H} = 1.22$ Hz, 1H), 8.34 (s, 1H), 8.62 (s, 1H), 8.82 (d, $^3J_{H,H} = 8.54$ Hz, 1H). ^{13}C NMR (DMSO-d_6): $\delta = 19.51$, 33.90, 112.76, 117.85, 121.68, 124.90, 125.62, 125.70, 126.14, 128.23, 129.09, 129.91, 132.67, 136.04, 139.90, 147.76, 151.34, 158.94. Electronic spectrum in CH_3CN: absorption, λ_{max} (nm) = 297, 363, 410; emission, λ_{max} (nm) = 641.

4.6.5. fac-Re(mqbO)(CO)$_3$Cl (**5**)

Yield: 76%. Anal. Calc. for $C_{20}H_{12}Cl_1N_2O_4Re_1$ (565.99): C, 42.44; H, 2.14; N, 4.95. Found: C, 42.48; H, 1.96; N, 4.81%. IR (KBr pellets, cm^{-1}): 1895 (s), 1923 (s), 2018 (s). ^{1}H NMR ($CDCl_3$): $\delta = 2.98$ (s, 3H), 7.67–7.70 (m, 2H), 7.79–7.82 (m, 1H), 7.88 (td, $^3J_{H,H} = 8.18$ Hz, $^4J_{H,H} = 0.98$ Hz, 1H), 8.08 (td, $^3J_{H,H} = 8.54$ Hz, $^4J_{H,H} = 1.34$ Hz, 1H), 8.18–8.21 (m, 2H), 8.24 (s, 1H), 8.96 (d, $^3J_{H,H} = 8.91$ Hz, 1H). ^{13}C NMR ($CDCl_3$): $\delta = 19.79$, 112.25, 120.35, 120.79, 125.06, 125.09, 127.83, 129.08, 130.19, 129.08, 130.97, 133.29, 144.84, 145.88, 147.82, 151.00. Electronic spectrum in CH_3CN: absorption, λ_{max} (nm) = 295, 343, 357, 400.

4.6.6. fac-Re(mqbS)(CO)$_3$Cl (**6**)

Yield: 86%. IR (KBr pellets, cm^{-1}): 1928 (m), 2018 (s). ^{1}H NMR ($CDCl_3$): $\delta = 2.92$ (s, 3H), 7.70 (t, $^3J_{H,H} = 7.93$ Hz, 1H), 7.81–7.85 (m, 2H), 8.02 (s, 1H), 8.04–8.07 (m, 2H), 8.15 (d, $^3J_{H,H} = 8.30$ Hz, 1H), 8.64 (d, $^3J_{H,H} = 8.38$ Hz, 1H), 8.64 (d, $^3J_{H,H} = 8.18$ Hz, 1H), 8.99 (d, $^3J_{H,H} = 9.15$ Hz, 1H). ^{13}C NMR ($CDCl_3$): $\delta = 19.77$, 121.35, 122.72, 124.42, 125.55, 124.88, 128.69, 129.47, 129.34, 129.84, 131.36, 133.20, 150.62, 150.69, 152.48, 152.98, 163.14. Electronic spectrum in CH_3CN: absorption, λ_{max} (nm) = 298, 354, 372, 415. MS (EI): *m*/*z* 582 $[M]^+$.

4.7. General synthesis of fac-[Re(N–N)(CO)$_3$(py)]PF$_6$

A mixture of *fac*-Re(N–N)(CO)$_3$Cl and $AgNO_3$ (20% excess) in CH_3CN was heated to reflux, in the dark, under nitrogen atmosphere for 8 h. The resulting mixture was cooled to room temperature and the precipitated AgCl was removed by filtration. The rhenium complex was then precipitated from the resulting solution as hexafluorophosphate salt by adding an aqueous solution of NH_4PF_6 and removing the acetonitrile by evaporation under vacuum.

The [Re(N–N)(CO)$_3$CH$_3$CN]PF$_6$ derivative obtained was heated to reflux in THF with an excess of pyridine (py) (30:1) under nitrogen atmosphere for 2 h. The resulting solution was cooled to room temperature and the complex was precipitate adding pentane and then filtered.

4.7.1. fac-[Re(mpbN)(CO)$_3$(py)]PF$_6$ (**7**)

Yield: 53%. Anal. Calc. for $C_{22}H_{18}F_6N_4O_3P_1Re_1$ (717.58): C, 36.82; H, 2.53; N, 7.81. Found: C, 35.16; H, 2.63; N, 7.38%. IR (KBr pellets, cm^{-1}): 1908 (m), 2027 (s). ^{1}H NMR (acetone-d_6): $\delta = 2.70$ (s, 3H), 4.51 (s, 1H), 7.41 (t, $^3J_{H,H} = 6.5$ Hz, 2H), 7.75–7.79 (m, 2H), 7.88 (d, $^3J_{H,H} = 5.6$ Hz, 1H), 7.96 (t, $^3J_{H,H} = 7.7$ Hz, 1H), 8.05 (d, $^3J_{H,H} = 7.3$ Hz, 1H), 8.17 (d, $^3J_{H,H} = 7.1$ Hz, 1H), 8.47 (d, $^3J_{H,H} = 5.0$ Hz, 2H), 8.68 (s, 1H), 9.42 (d, $^3J_{H,H} = 5.7$ Hz, 1H). ^{13}C NMR (acetone-d_6): $\delta = 21.70$, 34.21, 113.50, 118.77, 127.40, 127.67, 127.71, 130.48, 137.74, 140.60, 140.79, 147.98, 153.25, 155.00, 155.51, 155.62. Electronic spectrum in CH_3CN: absorption, λ_{max} (nm) = 282, 330, 366; emission, λ_{max} (nm) = 565.

4.7.2. fac-[Re(mpbO)(CO)$_3$(py)]PF$_6$ (**8**)

Yield: 62%. IR (KBr pellets, cm^{-1}): 1910 (s), 1928 (s), 2026 (s). ^{1}H NMR (acetone-d_6): $\delta = 2.73$ (s, 3H), 7.46 (t, $^3J_{H,H} = 7.3$ Hz, 1H), 7.43 (t, $^3J_{H,H} = 7.1$ Hz, 2H), 7.87–7.94 (m, 2H), 7.98 (t, $^3J_{H,H} = 7.7$ Hz, 1H), 8.04 (d, $^3J_{H,H} = 5.6$ Hz, 1H), 8.08 (d, $^3J_{H,H} = 7.4$ Hz, 1H), 8.24 (d, $^3J_{H,H} = 7.8$ Hz, 1H), 8.49 (s, 1H), 8.61 (d, $^3J_{H,H} = 5.1$ Hz, 2H), 9.45 (d, $^3J_{H,H} = 5.7$ Hz, 1H). ^{13}C NMR (acetone-d_6): 21.51, 113.83, 119.52, 127.84, 127.84, 130.44, 132.65, 138.93, 144.60, 152.22, 153.81, 155.72, 156.16. Electronic spectrum in CH_3CN: absorption, λ_{max} (nm) = 315, 328, 370; emission, λ_{max} (nm) = 610. MS (ESI): *m*/*z* 560 [M]$^+$.

4.7.3. fac-[Re(mpbS)(CO)$_3$(py)]PF$_6$ (**9**)

Yield: 51%. Anal. Calc. for $C_{21}H_{15}F_6N_3O_3P_1Re_1S$ (720.60): C, 35.00; H, 2.10; N, 5.83. Found: C, 34.16; H, 2.03; N, 5.65%. IR (KBr pellets, cm^{-1}): 1915 (m), 2030 (s). ^{1}H NMR (acetone-d_6): $\delta = 2.68$ (s, 3H), 7.43 (t, $^3J_{H,H} = 7.1$ Hz, 1H), 7.88 (d, $^3J_{H,H} = 5.6$ Hz, 1H), 7.90–8.00 (m, 3H), 8.09 (t, $^3J_{H,H} = 7.9$ Hz, 1H), 8.44 (d, $^3J_{H,H} = 5.0$ Hz, 2H), 8.50 (d, $^3J_{H,H} = 7.9$ Hz, 1H), 8.56 (s, 1H), 8.66 (d, $^3J_{H,H} = 8.4$ Hz, 1H), 9.44 (d, $^3J_{H,H} = 5.6$ Hz, 1H). ^{13}C NMR (acetone-d_6): 21.75, 122.51, 124.50, 127.15, 127.44, 129.16, 130.24, 131.09, 133.95, 140.24, 150.90, 151.37, 152.55, 153.81, 21.70, 155.42, 173.01. Electronic spectrum in CH_3CN: absorption, λ_{max} (nm) = 283, 334, 343, 380; emission, λ_{max} (nm) = 620.

4.7.4. fac-[Re(mqbN)(CO)$_3$(py)]PF$_6$ (**10**)

Yield: 49%. IR (KBr pellets, cm^{-1}): 1938 (m), 2029 (s). ^{1}H NMR (DMSO-d_6): $\delta = 3.08$ (s, 3H), 4.59 (s, 3H), 7.27 (t, $^3J_{H,H} = 6.59$ Hz, 2H), 7.78–7.85 (m, 2H), 7.90 (td, $^3J_{H,H} = 8.36$ Hz, $^4J_{H,H} = 1.34$ Hz, 1H), 8.01 (d, $^3J_{H,H} = 5.74$ Hz, 2H), 8.07–8.11 (m, 2H), 8.29–8.35 (m, 2H), 8.52 (d, $^3J_{H,H} = 8.42$ Hz, 1H), 8.69 (s, 1H), 9.08 (d, $^3J_{H,H} = 9.03$ Hz, 1H). ^{13}C NMR (DMSO-d_6): $\delta = 19.51$, 33.90, 113.74, 118.97, 122.89, 126.98, 127.69, 127.75, 126.14, 128.23, 129.09, 129.91, 132.67, 136.04, 139.90, 147.76, 151.34, 158.94. Electronic spectrum in CH_3CN: absorption, λ_{max} (nm) = 299, 363, 410; emission, λ_{max} (nm) = 625. MS (ESI): *m*/*z* 623 [M]$^+$.

4.7.5. fac-[Re(mqbO)(CO)$_3$(py)]PF$_6$ (**11**)

Yield: 65%. Anal. Calc. for $C_{25}H_{17}F_6N_3O_4P_1Re_1$ (754.5997832): C, 39.79; H, 2.27; N, 5.57. Found: C, 39.74; H, 2.27; N, 5.58%. IR (KBr pellets, cm^{-1}): 1918 (s), 1943 (s), 2035 (s). ^{1}H NMR (DMSO-d_6): $\delta = 2.87$ (s, 3H), 7.33 (t, $^3J_{H,H} = 7.02$ Hz, 2H), 7.87–8.02 (m, 4H), 8.08–8.19 (m, 3H), 8.31 (d, $^3J_{H,H} = 5.12$ Hz, 2H), 8.38–8.45 (m, 1H), 8.55 (s, 1H), $\delta = 9.09$ (d, $^3J_{H,H} = 8.54$ Hz, 1H). ^{13}C NMR (DMSO-d_6): $\delta = 19.67$, 113.99, 119.75, 122.64, 127.59, 128.01, 129.44, 129.85, 131.91, 130.87, 131.79, 135.61, 139.51, 141.00, 143.33, 146.46, 147.98, 152.22, 153.67, 155.27. Electronic spectrum in CH_3CN: absorption, λ_{max} (nm) = 298, 344, 380; emission, λ_{max} (nm) = 635.

4.7.6. fac-[Re(mqbS)(CO)$_3$(py)]PF$_6$ (**12**)

Yield: 58%. IR (KBr pellets, cm^{-1}): 1928 (m), 2030 (s). ^{1}H NMR (acetonitrile-d_3): $\delta = 2.92$ (s, 3H), 7.37 (t, $^3J_{H,H} = 6.71$ Hz, 2H), 7.73–7.80 (m, 1H), 7.87 (t, $^3J_{H,H} = 7.69$ Hz, 1H), 8.00–8.04 (m, 2H), 8.17 (s, 1H), 8.25 (t,d, $^3J_{H,H} = 8.60$ Hz, $^4J_{H,H} = 1.40$ Hz, 1H), 8.34–8.41 (m, 2H), 8.57 (d, $^3J_{H,H} = 8.42$ Hz, 1H), 8.70 (d, $^3J_{H,H} = 8.54$ Hz, 1H), $\delta = 8.99$ (d, $^3J_{H,H} = 8.91$ Hz, 1H). ^{13}C NMR (acetonitrile-d_3): $\delta = 19.54$, 123.01, 123.72, 124.99, 125.23, 127.25, 127.80, 130.23, 130.50, 130.60, 132.44, 135.02, 135.38, 137.54, 138.55, 140.94, 150.51, 152.51, 157.64. Electronic spectrum in CH_3CN: absorption, λ_{max} (nm) = 301, 360, 373, 405; emission, λ_{max} (nm) = 660. MS (ESI): *m*/*z* 626 [M]$^+$.

Acknowledgements

C.G. and R.B. thank the Regione Piemonte for a Grant (Project No. 111/10277). G.V. and R.B. thank Compagnia di San Paolo and Fondazione CRT, Torino Italy for continuous equipment supply. Support for this research by the Department of Energy (E.R., Grant DE-FG02-01ER45869) and Italian MIUR.

Appendix A. Supplementary material

Calculated and experimental absorption spectra and EDDMs of the MLCT transitions for complexes **1**–**6** and **10**–**12**. Curves were obtained using the program package GAUSSSUM 1.0. The Crystallographic Information File (CIF) has been deposited by the Cambridge Crystallographic Data Centre. CCDC 622255 and 622256 contain the supplementary crystallographic data for **1** and **7**. These data can be obtained free of charge via http://www.ccdc.cam.ac.uk/conts/retrieving.html, or from the Cambridge Crystallographic Data Centre, 12 Union Road, Cambridge CB2 1EZ, UK; fax: (+44) 1223-336-033; or e-mail: deposit@ccdc.cam.ac.uk. Supplementary data associated with this article can be found, in the online version, at doi:10.1016/j.jorganchem.2006.11.004.

References

[1] J.R. Lakowicz, Principles of Fluorescence Spectroscopy, second ed., Kluwer Academic/Plenum Publishers, New York, 1999.
[2] J.N. Demas, B.A. DeGraff, Coord. Chem. Rev. 211 (2001) 317–351.
[3] M.H. Keefe, K.D. Benkstein, J.T. Hupp, Coord. Chem. Rev. 205 (2000) 201–228.
[4] G.R. Haugen, F.E. Lytle, Anal. Chem. 53 (1981) 1554–1559.
[5] M.G. Grätzel, Energy Resources Through Photochemistry and Catalysis, Academic Press, New York, 1983.
[6] M.K. Nazeeruddin, R. Humphry-Baker, M.G. Grätzel, B.A. Murrer, Chem. Commun. (1998) 719–720.
[7] S.M. Zakeeruddin, M.K. Nazeeruddin, R. Humphry-Baker, M.G. Grätzel, V. Shklover, Inorg. Chem. 37 (1998) 5251–5259.
[8] Y. Jenkins, A.E. Friedman, N.J. Turro, J.K. Barton, Biochemistry 31 (1992) 10809–10816.
[9] C. Turro, S.H. Bossmann, Y. Jenkins, J.K. Barton, N.J. Turro, J. Am. Chem. Soc. 117 (1995) 9026–9032.
[10] I. Haq, P. Lincoln, D.C. Suh, B. Norden, B.Z. Chowdhry, J.B. Chaires, J. Am. Chem. Soc. 117 (1995) 4788–4796.
[11] V. Balzani, F. Bolletta, M. Gandolfi, M. MaestriTopics in Current Chemistry, vol. 75, Springer, Berlin/Heidelberg, 1978.
[12] A. Juris, V. Balzani, F. Barigelletti, S. Campagna, P. Belser, A. von Zelewsky, Coord. Chem. Rev. 84 (1988) 85–277.
[13] K. Kalyanasundaram, Coord. Chem. Rev. 46 (1982) 159–244.
[14] C. Garino, S. Ghiani, R. Gobetto, C. Nervi, L. Salassa, V. Ancarani, P. Neyroz, L. Franklin, J.B.A. Ross, E. Seibert, Inorg. Chem. 44 (2005) 3875–3879.
[15] R. Gobetto, G. Caputo, C. Garino, S. Ghiani, C. Nervi, L. Salassa, E. Rosenberg, J.B.A. Ross, G. Viscardi, G. Martra, I. Miletto, M. Milanesio, Eur. J. Inorg. Chem. (2006) 2839–2849.
[16] P.G. Sammes, G. Yahioglu, Nat. Prod. Rep. 13 (1996) 1–28.
[17] X.Q. Guo, F.N. Castellano, L. Li, J.R. Lakowicz, Anal. Chem. 70 (1998) 632–637.
[18] X.Q. Guo, F.N. Castellano, L. Li, H. Szmacinski, J.R. Lakowicz, J. Sipior, Anal. Biochem. 254 (1997) 179–186.
[19] J.D. Dattelbaum, O.O. Abugo, J.R. Lakowicz, Bioconjugate Chem. 11 (2000) 533–536.
[20] T.R. Harkins, J.L. Walter, O.E. Harris, H.J. Freiser, J. Am. Chem. Soc. 78 (1956) 260–264.
[21] B. Chiswell, F. Lions, B.S. Morris, Inorg. Chem. 3 (1964) 110–114.
[22] X.Y. Chen, F.J. Femia, J.W. Babich, J. Zubieta, Inorg. Chim. Acta 314 (2001) 91–96.
[23] K.Z. Wang, L. Huang, L.H. Gao, L.P. Jin, C.H. Huang, Inorg. Chem. 41 (2002) 3353–3358.
[24] N.M. Shavaleev, Z.R. Bell, T.L. Easun, R. Rutkaite, L. Swanson, M.D. Ward, Dalton Trans. (2004) 3678–3688.
[25] V. Balzani, F. Scandola, Supramolecular Photochemistry, Ellis-Horwood, Chichester, UK, 1991.
[26] R. Czerwieniec, A. Kapturkiewicz, J. Lipkowski, J. Nowacki, Inorg. Chim. Acta 358 (2005) 2701–2710.
[27] J.V. Caspar, T.J. Meyer, J. Phys. Chem. A 87 (1983) 952–957.
[28] S.R. Stoyanov, J.M. Villegas, A.J. Cruz, L.L. Lockyear, J.H. Reibenspies, D.P. Rillema, J. Chem. Theor. Comput. 1 (2005) 95–106.
[29] M. Leirer, G. Knor, A. Vogler, Inorg. Chim. Acta 288 (1999) 150–153.
[30] J.M. Villegas, S.R. Stoyanov, W. Huang, L.L. Lockyear, J.H. Reibenspies, D.P. Rillema, Inorg. Chem. 43 (2004) 6383–6396.
[31] M.M. Richter, Chem. Rev. 104 (2004) 3003–3036.
[32] W.L. Wallace, A.J. Bard, J. Phys. Chem. 83 (1979) 1350–1357.
[33] A.D. Becke, J. Chem. Phys. 98 (1993) 5648–5652.
[34] C. Lee, W. Yang, R.G. Parr, Phys. Rev. B 37 (1988) 785–789.
[35] M.J. Frisch, G.W. Trucks, H.B. Schlegel, G.E. Scuseria, M.A. Robb, J.R. Cheeseman, J.A. Montgomery Jr., T. Vreven, K.N. Kudin, J.C. Burant, J.M. Millam, S.S. Iyengar, J. Tomasi, V. Barone, B. Mennucci, M. Cossi, G. Scalmani, N. Rega, G.A. Petersson, H. Nakatsuji, M. Hada, M. Ehara, K. Toyota, R. Fukuda, J. Hasegawa, M. Ishida, T. Nakajima, Y. Honda, O. Kitao, H. Nakai, M. Klene, X. Li, J.E. Knox, H.P. Hratchian, J.B. Cross, C. Adamo, J. Jaramillo, R. Gomperts, R.E. Stratmann, O. Yazyev, A.J. Austin, R. Cammi, C. Pomelli, J. Ochterski, P.Y. Ayala, K. Morokuma, G.A. Voth, P. Salvador, J.J. Dannenberg, V.G. Zakrzewski, S. Dapprich, A.D. Daniels, M.C. Strain, O. Farkas, D.K. Malick, A.D. Rabuck, K. Raghavachari, J.B. Forestman, J.V. Ortiz, Q. Cui, A.G. Baboul, S. Clifford, J. Cioslowski, B.B. Stefanov, G. Liu, A. Liashenko, P. Piskorz, I. Komaromi, R.L. Martin, D.J. Fox, T. Keith, M.A. Al-Laham, C.Y. Peng, A. Nanayakkara, M. Challacombe, P.M.W. Gill, B. Johnson, W. Chen, M.W. Wong, C. Gonzales, J.A. Pople, GAUSSIAN-03, Rev. C.02, Gaussian, Inc., Wallingford, CT, 2004.
[36] D. Andrae, U. Haussermann, M. Dolg, H. Stoll, H. Preuss, Theor. Chim. Acta 77 (1990) 123–141.
[37] W.R. Browne, N.M. O'Boyle, J.J. McGarvey, J.G. Vos, Chem. Soc. Rev. 34 (2005) 641–663.
[38] V. Barone, M. Cossi, J. Phys. Chem. A 102 (1998) 1995–2001.
[39] M. Cossi, N. Rega, G. Scalmani, V. Barone, J. Comput. Chem. 24 (2003) 669–681.
[40] M. Cossi, V. Barone, J. Chem. Phys. 115 (2001) 4708–4717.
[41] N.M. O'Boyle, J.G. Vos. GAUSSSUM [1.0], Dublin City University, 2005.
[42] J.M. Villegas, S.R. Stoyanov, J.H. Reibenspies, D.P. Rillema, Organometallics 24 (2005) 395–404.
[43] M.K. Nazeeruddin, F. De Angelis, S. Fantacci, A. Selloni, G. Viscardi, P. Liska, S. Ito, B. Takeru, M.G. Grätzel, J. Am. Chem. Soc. 127 (2005) 16835–16847.
[44] J.B. Forestman, Æ. Frisch, Exploring Chemistry with Electronic Structure methods, second ed., Gaussian, Inc., Pittsburgh, PA, 1996.
[45] D.M. Dattelbaum, R.L. Martin, J.R. Schoonover, T.J. Meyer, J. Phys. Chem. A 108 (2004) 3518–3526.
[46] L.F. Amarengo, C. Chai, Purification of Laboratory Chemicals, fifth ed., Elsevier, Amsterdam, 2003.
[47] R.E. Stratmann, G.E. Scuseria, M.J. Frisch, J. Chem. Phys. 109 (1998) 8218–8224.
[48] M.E. Casida, C. Jamorski, K.C. Casida, D.R. Salahub, J. Chem. Phys. 108 (1998) 4439–4449.
[49] M.C. Burla, M. Camalli, B. Carrozzini, G.L. Cascarano, C. Giacovazzo, G. Polidori, R. Spagna, J. Appl. Crystallogr. 36 (2003) 1103.
[50] G.M. Sheldrick, SHELXL-97, University of Göttingen, Göttingen, Germany, 1997.
[51] E. Barni, P. Savarino, J. Heterocycl. Chem. 14 (1977) 937–940.
[52] E. Barni, C. Barolo, P. Quagliotto, P. Savarino, G. Viscardi, D. Marabello, J. Heterocycl. Chem. 40 (2003) 649–654.